J Eng Math (2008) 62:247–259
DOI 10.1007/s10665-007-9205-z

Natural convection in horizontal annuli: a lower bound for the energy

Arianna Passerini · Carlo Ferrario · Gudrun Thäter

Received: 8 January 2007 / Accepted: 23 October 2007 / Published online: 22 November 2007

Abstract Natural convection in the gap between two infinitely long horizontal coaxial cylindrical surfaces, each of which is maintained at constant temperature, is studied. If the inverse relative gap width $\mathcal{A}$ is large, relevant steady convective flow and considerable heat transfer are observed, even for extremely small Rayleigh numbers Ra. A lower bound for the norm of the velocity and of the temperature is rigorously found by studying an approximation problem, which is a good model in the parameter range where steady stable flow occurs. The lower bound depends on $\mathcal{A}$ only, and is an increasing function of $\mathcal{A}$. This means that the bound can be arbitrarily increased via the geometry only, no matter how small the temperature difference is, and independently of the Prandtl number Pr.

Keywords Inverse relative gap width · Nusselt number · Oberbeck–Boussinesq approximation · Prandtl number · Rayleigh number

1 Introduction

Natural convection of Newtonian fluid in an infinitely long gap between two cylinders whose common axis is horizontal, has been extensively investigated. It has a wide range of applications such as thermal storage plants, thermal insulation and cooling systems. It can be studied to understand the heat transfer in such different objects, such as nuclear reactors, electrical gas-insulated transmission lines or solar concentrators.

The energy considerations which are necessary in technology usually follow from a knowledge of the heat transfer, represented by the Nusselt number. Although in the spatial configuration considered here, rigorous theoretical estimates of the average Nusselt number are seldom provided, they can be found, for instance, in [1–3] for turbulent convection and in [4,5] for laminar flows.

A. Passerini
Dipartimento di Ingegneria, Università di Ferrara, Via Saragat, 1, 4410 Ferrara, Italy

C. Ferrario
Dipartimento di Fisica e Sezione INFN, Università di Ferrara, Via Saragat, 1, 44100 Ferrara, Italy

G. Thäter (✉)
Fachbereich Mathematik, Universität Dortmund, 44221 Dortmund, Germany
e-mail: gudrun.theater@uni-dortmund.de

A comprehensive review of the available *experimental* data and *numerical* results for heat transfer in a horizontal circular annulus has been presented by Teertstra and Yovanovich [6]. In that paper, the problem is analyzed in terms of the average Nusselt number, expressed as a function of the aspect ratio R_o/R_i and of the Rayleigh number Ra.

The average heat-transfer rate in the annulus shows two limiting cases. First, at large Rayleigh numbers and large aspect ratios a boundary-layer behavior occurs. In this region the average Nusselt number shows a strong dependence on Ra, but a somewhat weaker dependence on the aspect ratio, because of the relative unimportance of the outer boundary for large aspect ratios. Second, for small values of Ra or of the aspect ratio, the average Nusselt number shows a strong dependence on the aspect ratio, while it is almost independent of Ra.

Also, the flow patterns observed in the horizontal circular annulus have been classified by Powe et al. [7]. Depending on the Rayleigh number and the inverse relative gap width $\mathcal{A} := 2R_i/(R_o - R_i)$ they found four basic types of flow. For sufficiently small Rayleigh numbers and for any inverse relative gap width $\mathcal{A}$, the flow observed is a steady 2d one, with two crescent-shaped eddies which are symmetric with respect to the vertical plane through the common axis of the cylinders. As the Rayleigh number increases above a critical value, different unsteady flow patterns were observed: 2d oscillatory flow for $\mathcal{A} < 2.8$ (wide gap), 3d spiral flow for $2.8 < \mathcal{A} < 8.5$, 2d multi-cellular flow for $\mathcal{A} > 8.5$ (narrow gap).

The flow pattern was examined closely later by other authors; see, in particular; Yoo [8–10]. This author reports that, if the Rayleigh number is greater than a certain critical value, dual steady solutions are realized in the flow regime in which Powe et al. [7] asserts that a steady 2d flow prevails. One solution corresponds to the commonly observed uni-cellular crescent-shaped pattern in which the fluid ascends along the central plane (the inner cylinder is kept hotter). The other is a flow consisting of two counter-rotating eddies and their mirror image.

Moreover, in the narrow gap region (large $\mathcal{A}$) a further transition to multi-cellular steady flows is again observed by Yoo. Thus, this region of the parameter range has been thoroughly investigated lately (see [11,12] and related references), since the flow of thin films shows an interesting Bénard-like behavior on the top of the annulus. One could think of such phenomena as being due to the small curvature, which approximates the limiting case of parallel planes. In particular, at the bottom of the domain the fluid is almost at rest, since the decrease in temperature occurs in a direction opposite to that of the buoyancy force.

In the light of the previous observations, what should be expected for large $\mathcal{A}$ is a consistent convective flow, with a fairly articulated streamline structure, as noticed in [9–12], associated with a consistent average Nusselt number, strongly depending on $\mathcal{A}$, as noticed in [6]. All these properties occur even for very small Rayleigh numbers, so small that one would observe the fluid almost at rest if $\mathcal{A}$ were also small. This would happen because, as shown in [4,5], the upper bound for the solutions (the one usually related to classical energy stability analysis as in [13, Sect. 54]) is of order Ra/b, where the parameter $b := \log(R_o/R_i) = \log(1 + 2/\mathcal{A})$ is large for small $\mathcal{A}$. Oppositely, in the region defined by $\mathrm{Ra} < 16$ but $\mathcal{A} > 8.5$, the upper bound for the solutions shows a non-negligible order of magnitude, since b vanishes as $\mathcal{A}$ tends to infinity.

The aim of the present paper is to achieve a more complete theoretical prediction of this behavior by providing estimates from below of the solutions of a simplified mathematical model. As a matter of fact, the presence of a body-force term suggests to resort, for a full explanation, to estimates of the lower bound. Actually, whenever a body force is present, some lower bound can always be expected, which is of particular interest in the case of turbulent flows (see [14, Sect. 10.3]).

2 Mathematical model

In the present spatial configuration the average Nusselt number is

$$\overline{\mathrm{Nu}} := \frac{R_o - R_i}{(T_o - T_i)\,|A|} \int_A \nabla T \cdot \mathbf{n}\, \mathrm{d}A\,, \tag{1}$$

where R_o and R_i are the outer and inner cylindrical radius, respectively, (see Fig. 1), while T_o and T_i (with $T_o < T_i$) are the uniform, fixed surface temperatures at the outer and the inner side, respectively, and $|A|$ stands for the

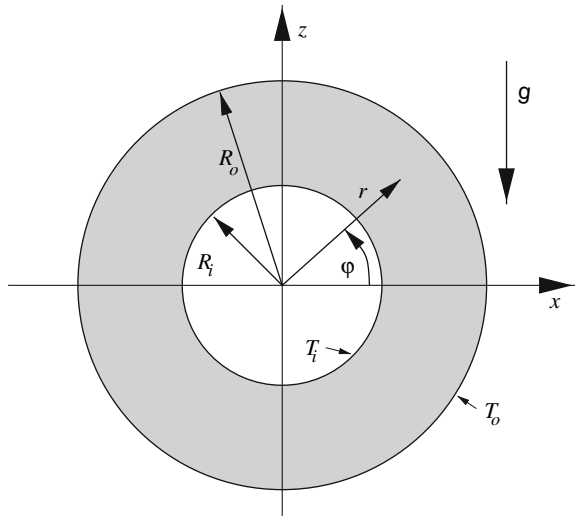

Fig. 1 2d-sketch of the domain in Cartesian and polar coordinates. The fluid moves in the shaded region under the combined effects of gravity g and of the temperature difference $T_i - T_o > 0$ between the surfaces

measure of either the inner or the outer surface, as we see fit. One sees from (1) that the magnitude of $\overline{\mathrm{Nu}}$ can be directly evaluated once the temperature distribution $T(\mathbf{x})$ is known pointwise.

In fact, the velocity field and temperature are usually found as the solution of a coupled system of partial differential equations, the Boussinesq system, representing an incompressible approximation (recently re-discussed in [15]) of the full Navier–Stokes–Fourier system. In the present paper, the solutions to Boussinesq's system of equations are replaced by solutions to a further approximation, already proposed in [5,16] and reconsidered here. Such a system, named *nonlinear Stokes problem*, is chosen in place of the fully linearized one, proposed in [17] and theoretically analyzed in [4], because the fully linearized model approximates the Nusselt number too roughly. In fact, it is proved that its solutions would produce the same $\overline{\mathrm{Nu}}$ as for pure conduction.

Actually, in the geometry given here the *theoretical* study of Boussinesq's system is a hard problem, due to the lack of symmetry in contrast to convective motions between parallel planes. This lack of symmetry results in a kind of body-force term. Moreover, contrary to the Bénard problem, it is impossible to solve the steady linearized problem with suitable couples of eigenfunctions of the Stokes and Laplace operators (given in [18]). This means that even the most simplified model problem for natural convection in horizontal annuli has not been solved analytically. Thus, in the domains we are considering, the analytical study of the dynamical system is still in an initial phase (see [19]).

Since all the published results [4,6–10] and references, indicate that for sufficiently small Ra, and independently of $\mathcal{A}$, a 2d *steady* flow is found, we write the steady version of the Boussinesq system. Moreover, to obtain dimensionless equations, we choose $L := R_o - R_i$ as typical length, $T_i - T_o$ as typical temperature, and L^2/κ as time scale, respectively. Notice that, choosing cylindrical coordinates, we have for the non-dimensional radius

$$r \in \left(\frac{\mathcal{A}}{2}, \frac{\mathcal{A}}{2} + 1\right). \tag{2}$$

Hence, the system is

$$\nabla \cdot \mathbf{v} = 0, \tag{3}$$

$$-\Delta \mathbf{v} + \nabla \Pi + \frac{1}{Pr}\, \mathbf{v} \cdot \nabla \mathbf{v} = \frac{\mathrm{Ra}}{b} \sin\varphi\, \mathbf{e}_r + \mathrm{Ra}\tau \nabla(r \sin\varphi), \tag{4}$$

$$\mathbf{v} \cdot \nabla \tau - \frac{v_r}{rb} = \Delta \tau\ , \tag{5}$$

where, as a consequence of the particular choice of dimensionless units, we have

$$\mathrm{Ra} := \frac{\alpha g}{\nu\kappa}(T_i - T_o)(R_o - R_i)^3, \quad \mathrm{Pr} := \frac{\nu}{\kappa}, \tag{6}$$

with α being volumetric expansion coefficient, g gravity acceleration, ν kinematic viscosity, and κ thermal diffusivity.

Moreover, the unknown τ is defined as follows

$$\tau := T - T^*, \quad \text{with} \quad T^* := \frac{T_i}{T_i - T_o} + \frac{\log R_i - \log r}{\log R_o - \log R_i}. \tag{7}$$

Thus, we study τ as relevant temperature (i.e., deviation from pure conduction) and, consequently, the boundary conditions for (3–5) are fully homogeneous:

$$v_r\left(\frac{\mathcal{A}}{2}, \varphi\right) = v_r\left(1 + \frac{\mathcal{A}}{2}, \varphi\right) = 0 \;\; v_\varphi\left(\frac{\mathcal{A}}{2}, \varphi\right) = v_\varphi\left(1 + \frac{\mathcal{A}}{2}, \varphi\right) = 0, \tag{8}$$

$$\tau\left(\frac{\mathcal{A}}{2}, \varphi\right) = \tau\left(1 + \frac{\mathcal{A}}{2}, \varphi\right) = 0\,. \tag{9}$$

Finally, all the functions must be periodic with respect to φ, otherwise the solution does not make sense physically.

In [19] it is shown that for sufficiently small Ra a solution can always be found for system (3–5). However, a simpler system would be easier to handle. In particular, we consider the nonlinear Stokes problem

$$\nabla \cdot \mathbf{w} = 0, \tag{10}$$

$$-\Delta \mathbf{w} + \nabla \Pi_0 = \frac{\mathrm{Ra}}{b} \sin\varphi\, \mathbf{e}_r + \mathrm{Ra}\tau_0 \nabla(r \sin\varphi), \tag{11}$$

$$\mathbf{w} \cdot \nabla \tau_0 - \frac{w_r}{rb} = \Delta \tau_0, \tag{12}$$

with boundary conditions (8–9) and periodicity conditions.

In [5], system (10–12) is studied as an approximation of (3–5) and the related *absolute error* is estimated. In particular, associated to the dimensionless domain

$$\Omega_{\mathcal{A}} := \{(r, \varphi) \in \mathbb{R}^2 : r \in (\mathcal{A}/2, 1 + \mathcal{A}/2)\,,\ \varphi \in (-\pi, +\pi)\}\,, \tag{13}$$

the L^2-scalar product and its derived norm, defined by

$$(\Psi, \Phi) := \int_{\Omega_{\mathcal{A}}} \Psi \cdot \Phi r \mathrm{d}r\mathrm{d}\varphi, \quad \|\Psi\|_2 := \sqrt{(\Psi, \Psi)}\,, \tag{14}$$

are considered. In (14), Ψ and Φ can be either scalar-, vector- or tensor-valued functions and the dot between Ψ and Φ denotes multiplication for scalar functions or the corresponding scalar product in case of vectors or tensors, respectively. Next, the norm of the difference between the gradients of solutions to problems (3–5) and (10–12), namely, the quantity $\|\nabla(\mathbf{v} - \mathbf{w})\|_2 + \|\nabla(\tau - \tau_0)\|_2$, is taken as a measure of the *absolute error*. Finally, an *upper bound* for the absolute error is found; such a bound essentially depends on $\mathrm{Pr}^{-1}(\mathrm{Ra}/b)^2$. Still in [5], the absolute error in the Nusselt number is of order $\mathrm{Pr}^{-1}(\mathrm{Ra}/b)^3$.

This is proved under an extremely restrictive condition on the range of Ra, due to the fact that Schwarz's inequality is too rough when dealing with coupling terms. By looking at Fig. 2, one can immediately see that the results in [5], although rigorous, are not of much use for applications. Anyway, the bottom line of those estimates is, that for *any* $\mathcal{A}$, the norm of the difference can be as small as we want, provided that Ra is sufficiently small or Pr sufficiently large.

In the present paper, we achieve, instead of the absolute error, an estimate of the *relative error* in the approximation. To get it, as we will see at the end of this section, a *lower bound* for the norm of the solutions is needed.

In Sect. 3, we provide the estimate of the lower bound for the L^2-norm of the solutions of (10–12) *without any restriction on the size of our dimensionless parameters*. To be more precise, what we find is a lower bound, depending on $\mathcal{A}$ only, for the sum of the kinetic energy (the L^2-norm of the velocity) and of the *non-conductive* thermal energy. With this last expression we mean the norm of τ, since T^* given in (7) is the temperature field

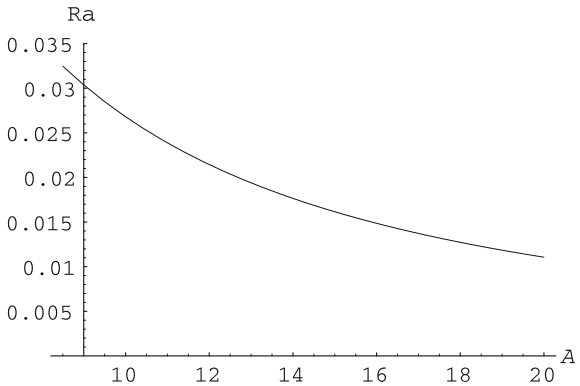

Fig. 2 The region below the line satisfies a sufficient condition to get both existence of solutions and estimates for the absolute error. This means that in such a region the relative error can be estimated

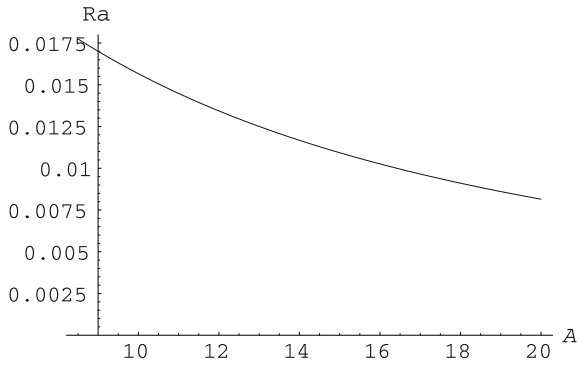

Fig. 3 In the region below the line the sufficient condition is fulfilled which ensures an approximation error less than 0.01

driven by pure conduction. Of course, a bound independent of Ra for steady solutions is an a priori bound, since for extremely large Ra steady solutions should not exist.

On the one hand, our lower bound can immediately be applied to check the accuracy of numerical simulations and, on the other hand, to estimate the relative error of (10–12) itself by the following scheme.

Let us consider system (10–12) and choose for its solution some norm Y, which we take as measure of the energy associated with the convective flow. Next, let us assume that one can estimate Y from below by

$$Y \geq f_1(\mathrm{Ra}, \mathcal{A}). \tag{15}$$

Further, let us indicate with ΔY the norm of the difference between solutions of (3–5) and (10–12). Assume that ΔY satisfies an estimate of the kind

$$\Delta Y \leq f_2(\mathrm{Ra}, \mathrm{Pr}, \mathcal{A}) \tag{16}$$

and let Y' be the norm of the solution of (3–5). Since the triangle inequality implies $Y' \geq Y - \Delta Y$, an estimate for the relative error η caused by the approximation is

$$\eta := \frac{\Delta Y}{Y'} \leq \frac{\Delta Y}{Y - \Delta Y} \leq \frac{f_2}{f_1 - f_2}\,. \tag{17}$$

Obviously, this is meaningful provided that $f_1 > f_2$.

In Sect. 4, we discuss how the estimate of the relative error confirms the validity of (10–12) as good approximation of the full problem. If $f_1 > f_2$, for any fluid, we can draw a region in (Ra, $\mathcal{A}$)-coordinates in which the nonlinear Stokes problem has a given precision as an approximation. In particular, after having deduced f_2 from the formerly discussed estimates available in [5], we draw, for air, a (non-optimal, of course!) region in which the accuracy is $\eta < 0.01$ (Fig. 3).

3 Estimates from below

Our main interest in this section is to quantify the distance of the flow from the rest state by energy estimates from below. They result from the presence of the term $(\mathrm{Ra}/b)\sin\varphi\,\mathbf{e}_r$ at the right-hand side of (11), which does not involve unknown fields, so that the system is not homogeneous and the rest state is never a solution. Thus, a lower bound for the solutions is just given by the square of the L_2-norm of that term. To minimize the errors in these estimates, we apply the Helmholtz decomposition [20, Sect. III.1],

$$\sin\varphi\,\mathbf{e}_r = \nabla\Phi + \boldsymbol{\Psi}, \tag{18}$$

in our non-dimensional domain $\Omega := \Omega_{\mathcal{A}}$, defined in (13). Its derivation and the exact expression of $\nabla\Phi$ can be found in Appendix 1 while the main property of the second term in (18) is, that div $\boldsymbol{\Psi} = 0$.

Besides, one calculates that $r\sin\varphi = z$ and $\nabla(r\sin\varphi) = \mathbf{k} = (0,1)^\top$. By directly substituting this and (18) in Eq. (11), we find

$$-\Delta\mathbf{w} + \nabla\left(\Pi_0 - \frac{\mathrm{Ra}}{b}\Phi\right) = \frac{\mathrm{Ra}}{b}\boldsymbol{\Psi} + \mathrm{Ra}\tau_0\mathbf{k}\,. \tag{19}$$

Then, the scalar product of (19) with $\boldsymbol{\Psi}$ in $L_2(\Omega)^3$ reads

$$-(\Delta\mathbf{w}, \boldsymbol{\Psi}) = \frac{\mathrm{Ra}}{b}\|\boldsymbol{\Psi}\|_2^2 + \mathrm{Ra}(\tau_0\mathbf{k}, \boldsymbol{\Psi})\,, \tag{20}$$

from which it immediately follows that

$$\frac{\mathrm{Ra}}{b}\|\boldsymbol{\Psi}\|_2^2 \le |(\Delta\mathbf{w}, \boldsymbol{\Psi})| + \mathrm{Ra}|(\tau_0\mathbf{k}, \boldsymbol{\Psi})|\,. \tag{21}$$

Now, let us prove that

$$(\Delta\mathbf{w}, \boldsymbol{\Psi}) = (\mathbf{w}, \Delta(\sin\varphi\,\mathbf{e}_r))\,. \tag{22}$$

By taking into account polar coordinates, the condition $\mathbf{w} = \mathbf{0}$ on $\partial\Omega$ in particular implies $\partial_\varphi\mathbf{w} = \mathbf{0}$ on the boundary (this is the tangential derivative on $\partial\Omega$ and we are dealing with smooth functions). Therefore, by the constraint

$$0 = \nabla\cdot\mathbf{w} = \partial_r w_r + \frac{w_r}{r} + \frac{1}{r}\partial_\varphi w_\varphi \tag{23}$$

it follows that also $\partial_r w_r = 0$ on the boundary.

Consequently, by the Gauss theorem together with the previous deductions as well as the orthogonality property related to (18) and the (obvious) property $\nabla\cdot\Delta\mathbf{w} = 0$, we can directly evaluate

$$\int_\Omega(\Delta\mathbf{w})\cdot\boldsymbol{\Psi} = \int_\Omega\left(\sum_i \partial_i\partial_i\mathbf{w}\right)\cdot\sin\varphi\,\mathbf{e}_r \tag{24}$$

$$= \int_{\partial\Omega}\sin\varphi\,\mathbf{n}\cdot(\nabla\mathbf{w}\cdot\mathbf{e}_r) - \int_\Omega\nabla\mathbf{w} : \nabla(\sin\varphi\,\mathbf{e}_r) \tag{25}$$

$$= \int_{\partial\Omega}\sin\varphi\,\mathbf{n}\cdot\left(\nabla w_r - \nabla\mathbf{e}_r\cdot\mathbf{w}\right) - \int_\Omega\nabla\mathbf{w} : \nabla(\sin\varphi\,\mathbf{e}_r) \tag{26}$$

$$= -\int_{\partial\Omega}\mathbf{n}\cdot(\nabla(\sin\varphi\,\mathbf{e}_r)\cdot\mathbf{w}) + \int_\Omega\Delta(\sin\varphi\,\mathbf{e}_r)\cdot\mathbf{w}, \tag{27}$$

$$= \int_\Omega\Delta(\sin\varphi\,\mathbf{e}_r)\cdot\mathbf{w}, \tag{28}$$

which proves Eq. (22) (it is understood that $\mathbf{n} = \pm\mathbf{e}_r$ depending on which part of the boundary is considered and we omit the obvious element of integration). Finally, (21) implies

$$\frac{\mathrm{Ra}}{b}\|\boldsymbol{\Psi}\|_2^2 \le \|\mathbf{w}\|_2\|\Delta(\sin\varphi\,\mathbf{e}_r)\|_2 + \mathrm{Ra}\|\tau_0\|_2\|\mathbf{k}\cdot\boldsymbol{\Psi}\|_2\,. \tag{29}$$

Now, from Appendices 1 and 2 we make use of the following results

$$(59) : \|\Delta(\sin\varphi\,\mathbf{e}_r)\|_2 = 8\frac{\sqrt{\pi(\mathcal{A}+1)}}{\mathcal{A}(\mathcal{A}+2)},$$

$$(69) : \|\boldsymbol{\Psi}\|_2^2 = \frac{\pi}{32(\mathcal{A}+1)}(36(\mathcal{A}+1)^2 - b^2\mathcal{A}^2(\mathcal{A}+2)^2),$$

$$(73) : \|\mathbf{k}\cdot\boldsymbol{\Psi}\|_2 = \sqrt{\frac{\pi}{32(\mathcal{A}+1)}\left(35(\mathcal{A}+1)^2 - 3\frac{b^2\mathcal{A}^2(\mathcal{A}+2)^2}{4}\right)}$$

to rewrite (29) as

$$\frac{\mathrm{Ra}}{b}\frac{\pi}{32(\mathcal{A}+1)}(36(\mathcal{A}+1)^2 - b^2\mathcal{A}^2(\mathcal{A}+2)^2) \le 8\frac{\sqrt{\pi(\mathcal{A}+1)}}{\mathcal{A}(\mathcal{A}+2)}\|\mathbf{w}\|_2 + \mathrm{Ra}\sqrt{\frac{\pi}{32(\mathcal{A}+1)}\left(35(\mathcal{A}+1)^2 - \frac{3b^2\mathcal{A}^2(\mathcal{A}+2)^2}{4}\right)}\|\tau_0\|_2 . \tag{30}$$

By comparing the coefficients at the right-hand side of (30) for large $\mathcal{A}$, since for any fixed Ra the coefficient of $\|\tau_0\|_2$ prevails provided $\mathcal{A}$ is sufficiently large, we get

$$\frac{2}{b}\sqrt{\frac{\pi}{32(\mathcal{A}+1)}}\frac{36(\mathcal{A}+1)^2 - b^2\mathcal{A}^2(\mathcal{A}+2)^2}{\sqrt{140(\mathcal{A}+1)^2 - 3b^2\mathcal{A}^2(\mathcal{A}+2)^2}} \le \|\mathbf{w}\|_2 + \|\tau_0\|_2 . \tag{31}$$

In order to understand the asymptotic behavior of the lower bound in (31), it is sufficient to point out that, as $\mathcal{A}$ tends to infinity, b tends to zero while $b\mathcal{A}$ tends to 2.

Inequality (31) shows that the intensity of the convective flow grows with $\mathcal{A}$. This growth has no upper bound, no matter how small the temperature difference is and independently of the Prandtl number. Obviously, one should ask whether, in such a situation, the internal dissipation can be neglected, and the Oberbeck–Boussinesq model is appropriate.

On the other hand, we proved this result by considering an approximation of the Oberbeck–Boussinesq model. In the next section, we show how (31) can be used to justify and *quantify* this approximation.

4 Evaluation of the error of the approximation

The region of the non-dimensional parameter range investigated in the present section is far from being optimal for any application. Nevertheless, since in the literature the approximations are usually considered without *theoretically quantifying* the related error, we like to present a region of the $(\mathcal{A}, \mathrm{Ra})$-plane, in which the natural convection of air ($\mathrm{Pr} = 0.7$) can be studied by means of the nonlinear Stokes problem (10–12) while the error is smaller than 0.01. With the same technique one can find the corresponding region for any fluid and any precision. Actually, we evaluate the error

$$\eta = \frac{\Delta Y}{Y'} := \frac{\|\mathbf{u}\|_2 + \|\sigma\|_2}{\|\mathbf{v}\|_2 + \|\tau\|_2} \tag{32}$$

with $\mathbf{u} := \mathbf{v} - \mathbf{w}$ and $\sigma := \tau - \tau_0$, where $(\mathbf{v}, \tau)$ and $(\mathbf{w}, \tau_0)$ are solutions of (3–5) and of (10–12), respectively. The gradients of the differences are estimated in [5], under a smallness condition on Ra.

By specifying the general considerations given in our introduction, we derive a bound for η. In doing this, we use the triangle as well as the Poincaré inequality

$$\|f\|_2 \le k_p\|\nabla f\|_2 , \tag{33}$$

which holds for any function f vanishing on the boundary for which the L_2-norm of ∇f is bounded. As proved in [4], the best general expression for the so-called Poincaré constant k_p in the region where $\mathcal{A}$ is large is

$$k_p^l = \frac{1}{2}\sqrt{1 + \frac{2}{\mathcal{A}}}. \tag{34}$$

Now, we can rewrite (32) as

$$\eta \le \frac{k_p^l(\|\nabla\mathbf{u}\|_2 + \|\nabla\sigma\|_2)}{\|\mathbf{w}\|_2 + \|\tau_0\|_2 - k_p^l(\|\nabla\mathbf{u}\|_2 + \|\nabla\sigma\|_2)} . \tag{35}$$

From (35) it immediately follows that if

$$\frac{k_p^l(\|\nabla \mathbf{u}\|_2 + \|\nabla \sigma\|_2)}{\|\mathbf{w}\|_2 + \|\tau_0\|_2} < \frac{1}{101}, \tag{36}$$

then $\eta < 0.01$. Thus, we will use (34) and suitable estimates in order to rewrite the left-hand side of (36) as a function of $\mathcal{A}$ and Ra, while $\mathrm{Pr} = 0.7$. Finally, we draw the curve for the upper bound of Ra satisfying (36).

However, in [5] the estimates for the gradients of the differences can be written only under a preliminary restrictive condition on Ra. In Appendix 3, after having recalled the existence conditions for solutions of system (3–5) [the same as for (10–12)], we show that estimates for the gradient of the difference between the solutions of the full system and the ones of the approximation system can be written when the following sufficient condition is satisfied

$$\mathrm{Ra} < \frac{28}{27} \frac{\log\left(1 + \frac{2}{\mathcal{A}}\right)}{\left(1 + \frac{2}{\mathcal{A}}\right)\sqrt{\pi}\sqrt{1+\mathcal{A}}}. \tag{37}$$

Condition (37) defines the region below the line in Fig. 2. By substituting in (36) the following estimates from [5]

$$\|\nabla \mathbf{u}\|_2 \leq \frac{1}{\alpha_0} \frac{(k_p^l)^3 \gamma^2}{\sqrt{2}\delta_0^2} \frac{1}{\mathrm{Pr}} \frac{\mathrm{Ra}^2}{b^2}, \tag{38}$$

$$\|\nabla \sigma\|_2 \leq \frac{1}{\alpha_0} \frac{\sqrt{2}(k_p^l)^5 \gamma^2}{\mathcal{A} b \delta_0^2} \left(1 + \frac{(k_p^l)^2 \mathrm{Ra}\gamma}{b\sqrt{2}\delta_0}\right) \frac{1}{\mathrm{Pr}} \frac{\mathrm{Ra}^2}{b^2}, \tag{39}$$

where α_0, δ_0 and γ (all equivalent to constants in the considered parameter range) are defined in Appendix 3, we see that the precision requirement (36) is satisfied if

$$\frac{f(\mathcal{A})\mathrm{Ra}^2}{7b - g(\mathcal{A})\mathrm{Ra}} - \frac{1}{101} < 0, \tag{40}$$

where

$$g(\mathcal{A}) := 27(k_p^l)^2 \sqrt{\pi(\mathcal{A}+1)} \tag{41}$$

and

$$f(\mathcal{A}) := \frac{160\sqrt{(\mathcal{A}+1)(140(\mathcal{A}+1)^2 - 3b^2\mathcal{A}^2(\mathcal{A}+2)^2)}}{\sqrt{\pi}(36(\mathcal{A}+1)^2 - b^2\mathcal{A}^2(\mathcal{A}+2)^2)\mathcal{A}b^2} \times (k_p^l)^4\gamma^2 \left(\mathcal{A}b^2 + \sqrt{2}(k_p^l)^2(\sqrt{2}b + 2(k_p^l)^2\gamma R^M)\right). \tag{42}$$

In the latter $R^M := 3.25 \times 10^{-2}$ corresponds to the maximum value of Ra in (37) which is attained for $\mathcal{A} = 8.5$. Condition (40) is nothing else than a sufficient condition for (36) and is introduced just to simplify some calculation.

The function $\mathrm{Ra}(\mathcal{A})$ defining the boundary of the 0.01-approximation region identified by (40–42) can be evaluated numerically since inequality (40) is equivalent to

$$\mathrm{Ra} < \frac{-g(\mathcal{A}) + \sqrt{g^2(\mathcal{A}) + 2828bf(\mathcal{A})}}{202 f(\mathcal{A})} \quad \text{and} \quad \mathrm{Ra} > 7\frac{b}{g(\mathcal{A})}. \tag{43}$$

The first condition in (43) gives rise to Fig. 3, which identifies a subset of the region depicted in Fig. 2 in which both steady solutions and estimates for the differences are available and, moreover, the error in the approximation is less than 0.01.

5 Concluding remarks

In the present paper, through a lower bound independent of Ra, we have described some particular features of natural convection in thin cylindrical gaps: in fact, for large $\mathcal{A}$, the convective flow is always rather consistent, even for small Ra, and several transitions to multicellular flow are observed.

To be more precise, by discussing (30) one sees that for any arbitrary $\mathrm{Ra}^* > 0$ a number $\overline{\mathcal{A}}(\mathrm{Ra}^*)$ can be found such that the steady solutions of the nonlinear Stokes problem satisfy the estimate (31) for all $\mathcal{A} > \overline{\mathcal{A}}(\mathrm{Ra}^*)$ and all $\mathrm{Ra} < \mathrm{Ra}^*$. Moreover, the lower bound in (31) increases with $\mathcal{A}$ and independent of Ra.

Our studies are, generally speaking, oriented to collect exact results on the dynamical system, in order to identify as much as possible the "size" and the features of the solutions, depending on the relevant dimensionless parameters. Of course, a big goal would be a mathematical characterization of the different transitions, allowing to predict the critical value of the parameters. But this can be done only through small steps.

At the moment, we think that with techniques similar to those of the present paper, a lower bound can be found in the 3d case as well as for the full Boussinesq system. Of course, here one has to find a way to treat the nonlinear term in the momentum equation and, in principle, a bound depending on Pr is expected.

Another interesting topic one may address, is the investigation of the large gap configuration, namely, the region given by small $\mathcal{A}$. In such a region the stable (observed) motions are still 2d and still steady, even for very large Ra. Then, one might try to consider a different approximation problem, the *decoupled problem* studied in [5], which has the desirable feature of allowing steady solutions in any region of the parameter space.

Such a system is obtained by leaving out the coupling term in the momentum equation. For small Ra, this is justified by realizing that the solution is small and, therefore, owing to multiplication by Ra, the coupling term is smaller (i.e., small in a nonlinear way).

Also, it is easy to show that any solution of the decoupled problem has the nature of an *upward flow*, similarly to the basic flow found in [8]. That flow is stable for values of Ra that are as large as we want provided $\mathcal{A}$ is small enough. Under this last condition a lower bound should be easily found.

Acknowledgements The authors thank the reviewers for valuable advice concerning the comprehensibility of the paper and cross-linking to other research. We are particularly grateful to the third one for very precise remarks showing an honest interest in our results.

Appendix 1: Helmholtz decomposition of the body force

Taking the divergence of the Helmholtz decomposition (18) gives rise to the Neumann problem

$$\nabla \cdot (\sin\varphi\, \mathbf{e}_r) = \Delta\Phi \quad \text{in } \Omega\,, \quad \nabla\Phi \cdot \mathbf{n} = 0 \quad \text{on } \partial\Omega\,, \tag{44}$$

where the condition $\nabla \cdot \mathbf{\Psi} = 0$ in Ω is used as well. Moreover, since

$$\nabla \cdot (\sin\varphi\, \mathbf{e}_r) = \frac{1}{r}\sin\varphi\,, \tag{45}$$

the above equation for Φ can be reduced to a second-order differential equation for $f(r)$, by the help of the ansatz

$$\Phi = f(r)\sin\varphi, \tag{46}$$

The result is

$$r^2 f'' + r f' - f = r\,, \tag{47}$$

which is an Euler–Cauchy equation whose general solution has the form

$$f(r) = C_1 r + \frac{C_2}{r} + \frac{r}{2}\log r\,. \tag{48}$$

By imposing the boundary condition $\nabla\Phi \cdot \mathbf{n} = 0$ on $\Phi = f\sin\varphi$, we find for the constants C_1 and C_2 the relations

$$C_1 - \frac{4C_2}{(\mathcal{A}+2)^2} + \frac{1}{2}\log\frac{\mathcal{A}+2}{2} + \frac{1}{2} = 0, \tag{49}$$

$$C_1 - \frac{4C_2}{\mathcal{A}^2} + \frac{1}{2}\log\frac{\mathcal{A}}{2} + \frac{1}{2} = 0\,. \tag{50}$$

Hence

$$C_1 = -\frac{b}{8}\frac{(\mathcal{A}+2)^2}{\mathcal{A}+1} - \frac{1}{2}\left(\log\frac{\mathcal{A}}{2}+1\right), \quad C_2 = -\frac{b}{32}\frac{\mathcal{A}^2(\mathcal{A}+2)^2}{\mathcal{A}+1}. \tag{51}$$

Consequently, for $\nabla\Phi$ and then for $\boldsymbol{\Psi}$ we calculate

$$\nabla\Phi = (\partial_r\Phi)\,\mathbf{e}_r + \left(\frac{1}{r}\partial_\varphi\Phi\right)\mathbf{e}_\varphi \tag{52}$$

$$= \left(C_1 - \frac{C_2}{r^2} + \frac{1}{2}\log r + \frac{1}{2}\right)\sin\varphi\,\mathbf{e}_r + \left(C_1 + \frac{C_2}{r^2} + \frac{1}{2}\log r\right)\cos\varphi\,\mathbf{e}_\varphi \tag{53}$$

$$\boldsymbol{\Psi} = \sin\varphi\,\mathbf{e}_r - \nabla\Phi \tag{54}$$

$$= \left(\frac{1}{2} - C_1 + \frac{C_2}{r^2} - \frac{1}{2}\log r\right)\sin\varphi\,\mathbf{e}_r - \left(C_1 + \frac{C_2}{r^2} + \frac{1}{2}\log r\right)\cos\varphi\,\mathbf{e}_\varphi\,. \tag{55}$$

Moreover, by taking into account $\mathbf{k} = \sin\varphi\mathbf{e}_r + \cos\varphi\mathbf{e}_\varphi$, we deduce

$$\boldsymbol{\Psi}\cdot\mathbf{k} = \left(\frac{1}{2} - C_1 + \frac{C_2}{r^2} - \frac{1}{2}\log r\right)\sin^2\varphi - \left(C_1 + \frac{C_2}{r^2} + \frac{1}{2}\log r\right)\cos^2\varphi \tag{56}$$

$$= -C_1 - \frac{1}{2}\log r - \frac{C_2}{r^2}\cos 2\varphi + \frac{1}{2}\sin^2\varphi\,. \tag{57}$$

In Appendix 2, we will calculate the L^2-norms of $\boldsymbol{\Psi}$ and of $\boldsymbol{\Psi}\cdot\mathbf{k}$. Moreover, in order to complete the analysis of inequality (29), we also have to evaluate the norm of

$$\Delta(\sin\varphi\,\mathbf{e}_r) = \frac{2}{r^2}(-\sin 2\varphi, \cos 2\varphi)^\top. \tag{58}$$

It is easy to see that

$$\int_\Omega |\Delta(\sin\varphi\,\mathbf{e}_r)|^2 r\mathrm{d}r\mathrm{d}\varphi = \int_{\frac{\mathcal{A}}{2}}^{\frac{\mathcal{A}+2}{2}}\int_{-\pi}^{\pi}\frac{4}{r^4}r\mathrm{d}r\mathrm{d}\varphi = 4\pi\left|-\frac{1}{r^2}\right|_{\frac{\mathcal{A}}{2}}^{1+\frac{\mathcal{A}}{2}} \tag{59}$$

$$= 64\pi\frac{(\mathcal{A}+1)}{\mathcal{A}^2(\mathcal{A}+2)^2}\,. \tag{60}$$

Appendix 2: Auxiliary calculations

In what follows, $\log\frac{\mathcal{A}+2}{2}$ will be replaced by $\left(b + \log\frac{\mathcal{A}}{2}\right)$. We calculate

$$\int_{\frac{\mathcal{A}}{2}}^{1+\frac{\mathcal{A}}{2}}\frac{1}{r}\mathrm{d}r = b, \quad \int_{\frac{\mathcal{A}}{2}}^{1+\frac{\mathcal{A}}{2}} r^2\mathrm{d}r = \mathcal{A}+1, \tag{61}$$

$$\int_{\frac{\mathcal{A}}{2}}^{1+\frac{\mathcal{A}}{2}}\frac{1}{r^3}\mathrm{d}r = \frac{8(\mathcal{A}+1)}{\mathcal{A}^2(\mathcal{A}+2)^2}, \tag{62}$$

$$\int_{\frac{\mathcal{A}}{2}}^{1+\frac{\mathcal{A}}{2}} r\log r\mathrm{d}r = \frac{1}{2}\left(\frac{\mathcal{A}^2}{4}b + (\mathcal{A}+1)\left(b+\log\frac{\mathcal{A}}{2}\right)\right) - \frac{1}{4}(\mathcal{A}+1), \tag{63}$$

$$\int_{\frac{\mathcal{A}}{2}}^{1+\frac{\mathcal{A}}{2}} r\log^2 r\mathrm{d}r = \frac{1}{2}\Big(\frac{\mathcal{A}^2 b}{4}\left(b+2\log\frac{\mathcal{A}}{2}\right)+(\mathcal{A}+1)\Big(b+\log\frac{\mathcal{A}}{2}\Big)^2\Big) \\ -\frac{1}{2}\left(\frac{\mathcal{A}^2 b}{4}+(\mathcal{A}+1)\left(b+\log\frac{\mathcal{A}}{2}\right)\right)+\frac{1}{4}(\mathcal{A}+1)\,. \tag{64}$$

We continue by computing

$$\boldsymbol{\Psi}\cdot\boldsymbol{\Psi} = \frac{C_2^2}{r^4}+\frac{1}{4}\log^2 r+2\frac{C_2}{r^2}\left(C_1+\frac{1}{2}\log r\right)\cos 2\varphi+\sin^2\varphi\left(\frac{1}{4}-C_1+\frac{C_2}{r^2}-\frac{1}{2}\log r\right)+C_1^2+C_1\log r, \tag{65}$$

$$\int_{-\pi}^{\pi}|\boldsymbol{\Psi}|^2\mathrm{d}\varphi = 2\pi\left(C_1^2+\frac{C_2^2}{r^4}+\frac{1}{4}\log^2 r+C_1\log r\right)+\pi\left(\frac{1}{4}-C_1+\frac{C_2}{r^2}-\frac{1}{2}\log r\right). \tag{66}$$

Consequently,

$$\|\boldsymbol{\Psi}\|_2^2 = \int_{\frac{\mathcal{A}}{2}}^{\frac{\mathcal{A}+2}{2}}\int_{-\pi}^{\pi} r|\boldsymbol{\Psi}|^2\mathrm{d}r\mathrm{d}\varphi \tag{67}$$

$$= \pi\left(2C_1^2+\frac{1}{4}-C_1\right)\frac{\mathcal{A}+1}{2}+\pi C_2 b+16\pi C_2^2\frac{\mathcal{A}+1}{\mathcal{A}^2(\mathcal{A}+2)^2}+ \\ +\pi\left(C_1-\frac{1}{4}\right)\left(\frac{\mathcal{A}^2}{4}b+(\mathcal{A}+1)\left(b+\log\frac{\mathcal{A}}{2}\right)-\frac{(\mathcal{A}+1)}{2}\right)+ \\ +\frac{\pi}{4}\left|r^2\log^2 r\right|_{\frac{\mathcal{A}}{2}}^{\frac{\mathcal{A}+2}{2}}-\frac{\pi}{4}\left(\frac{\mathcal{A}^2}{4}b+(\mathcal{A}+1)\left(b+\log\frac{\mathcal{A}}{2}\right)-\frac{(\mathcal{A}+1)}{2}\right). \tag{68}$$

After replacing C_1 and C_2 and another line of calculation, we have

$$\|\boldsymbol{\Psi}\|_2^2 = \frac{\pi}{8}\left(9(\mathcal{A}+1)-\frac{b^2\mathcal{A}^2(\mathcal{A}+2)^2}{4(\mathcal{A}+1)}\right). \tag{69}$$

Likewise, for $\int_{-\pi}^{\pi}(\boldsymbol{\Psi}\cdot\mathbf{k})^2\mathrm{d}\varphi =: I$, then

$$I = \pi\left(2C_1^2+\frac{\log^2 r}{2}+\frac{C_2^2}{r^4}+\frac{3}{16}-C_1+\left(2C_1-\frac{1}{2}\right)\log r+\frac{C_2}{2r^2}\right), \tag{70}$$

$$\frac{2}{\pi}\|\boldsymbol{\Psi}\cdot\mathbf{k}\|_2^2 = \left(2C_1^2-C_1+\frac{3}{16}\right)(\mathcal{A}+1)+C_2 b+\frac{16C_2^2(\mathcal{A}+1)}{\mathcal{A}^2(\mathcal{A}+2)^2} \\ +\left(2C_1-\frac{1}{2}\right)\left(\frac{\mathcal{A}^2}{4}b+(\mathcal{A}+1)\left(b+\log\frac{\mathcal{A}}{2}\right)-\frac{(\mathcal{A}+1)}{2}\right) \\ +\frac{1}{2}\left(\frac{\mathcal{A}^2}{4}b\left(b+2\log\frac{\mathcal{A}}{2}\right)+(\mathcal{A}+1)\left(b+\log\frac{\mathcal{A}}{2}\right)^2\right) \\ -\frac{1}{2}\left(\frac{\mathcal{A}^2}{4}b+(\mathcal{A}+1)\left(b+\log\frac{\mathcal{A}}{2}\right)-\frac{(\mathcal{A}+1)}{2}\right) \tag{71}$$

$$= \frac{b^2}{32}\frac{(\mathcal{A}+2)^4}{(\mathcal{A}+1)}+\frac{35}{16}(\mathcal{A}+1)+\frac{b}{2}(\mathcal{A}+2)^2-b^2\frac{\mathcal{A}^2(\mathcal{A}+2)^2}{64(\mathcal{A}+1)} \\ -b^2\frac{\mathcal{A}^2(\mathcal{A}+2)^2}{16(\mathcal{A}+1)}-\frac{\mathcal{A}^2}{4}b-\frac{b^2}{4}(\mathcal{A}+2)^2-b(\mathcal{A}+1) \\ -\frac{\mathcal{A}^2}{4}b-b(\mathcal{A}+1)+\frac{\mathcal{A}^2}{8}b^2+\frac{1}{2}(\mathcal{A}+1)b^2. \tag{72}$$

Hence, we obtain

$$\|\boldsymbol{\Psi}\cdot\mathbf{k}\|_2^2=\frac{\pi}{32(\mathcal{A}+1)}\left(35(\mathcal{A}+1)^2-3\frac{b^2\mathcal{A}^2(\mathcal{A}+2)^2}{4}\right). \tag{73}$$

Appendix 3: Necessary conditions for the existence of solutions

We now recall the results obtained in [5]. Let us start discussing the condition of existence for steady solutions of both (3–5) and (10–12): definition (2.3) in [5] implies that by choosing

$$\delta_0:=1-\frac{2(k_p^l)^4\mathrm{Ra}}{\mathcal{A}b}>\frac{1}{2}, \tag{74}$$

we find

$$\mathrm{Ra}<\frac{4\mathcal{A}^3}{(\mathcal{A}+2)^2}\log\left(1+\frac{2}{\mathcal{A}}\right), \tag{75}$$

and $\delta_0>0$ is the sufficient condition of existence. Next, we recall and discuss the sufficient condition allowing to write estimates for the difference of the two problems. For convenience we abbreviate $\gamma:=\sqrt{\pi\left(\frac{1+\mathcal{A}}{2}\right)}$. Then definition (2.12) in [5],

$$\alpha_0:=\delta_0-\frac{(k_p^l)^2}{b\sqrt{2}}\frac{\gamma}{\delta_0}\mathrm{Ra}\left(\frac{1}{\mathrm{Pr}}+1-\delta_0\right), \tag{76}$$

implies that if $\delta_0>\frac{1}{2}$ and $\mathrm{Pr}=0.7$, then the inequality

$$\alpha_0>\frac{1}{2}-\frac{27}{14}\left(1+\frac{2}{\mathcal{A}}\right)\frac{\sqrt{\pi}\sqrt{1+\mathcal{A}}}{4\log\left(1+\frac{2}{\mathcal{A}}\right)}\mathrm{Ra} \tag{77}$$

holds true for any values of $\mathcal{A}$ and Ra. The condition $\alpha_0>0$ allows to write the estimates for the differences. Then, α_0 is certainly positive if

$$\mathrm{Ra}<\frac{28}{27}\frac{\log\left(1+\frac{2}{\mathcal{A}}\right)}{\left(1+\frac{2}{\mathcal{A}}\right)\sqrt{\pi}\sqrt{1+\mathcal{A}}}. \tag{78}$$

The latter two inequalities together define a region in which the error can be estimated. Finally, since (75) is a weaker condition, we retain (78) only.

References

1. Constantin P, Doering CR (1996) Heat transfer in convective turbulence. Nonlinearity 9:1049–1060
2. Doering CR, Foias C (2002) Energy dissipation in body-forced turbulence. J Fluid Mech 467:289–306
3. Doering CR, Otto F, Reznikoff MG (2006) Bounds on vertical heat transport for infinite Prandtl number Rayleigh–Bénard convection. J Fluid Mech 560:229–241
4. Ferrario C, Passerini A, Piva S (2006) A Stokes-like system for natural convection in a horizontal annulus. Nonlinear Anal: Real World Appl, http://www.sciencedirect.com/science/article/B6W7S-4MS9R75-1/2/7be68db173dc60524162784a2a770c09
5. Duka B, Ferrario C, Passerini A, et al (2007) Non-linear approximation for natural convection in a horizontal annulus. Int J Non-Linear Mech 42(9):1055–1061
6. Teerstra P, Yovanovich MM (1998) Comprehensive review of natural convection in horizontal circular annuli. In: 7th AIAA/ASME joint thermophysics and heat transfer conference, 15–18 June 1998, Albuquerque, NM, HTD 357, p 141ff
7. Powe RE, Carley CT, Bishop EH (1969) Free convective flow patterns in cylindrical annuli. J Heat Transf 91:310–314
8. Yoo JS (1996) Natural convection in a narrow horizontal cylindrical annulus: $P_r\leq 0.3$. Int J Heat Fluid Flow 17:587–593
9. Yoo JS (1999) Transition and multiplicity of flows in natural convection in a narrow horizontal cylindrical annulus: $P_r=0.4$. Int J Heat Mass Transf 42:709–733

10. Yoo JS (1999) Prandtl number effect on bifurcation and dual solutions in natural convection in a horizontal annulus. Int J Heat Mass Transf 42:3279–3290
11. Mizushima J, Hayashy S (2001) Exchange of instability modes for natural convection in a narrow horizontal annulus. Phys Fluids 13:99–106
12. Mizushima J, Hayashy S, Adachi T (2001) Transition of natural convection in a horizontal annulus. Int J Heat Fluid Flow 44: 1249–1257
13. Joseph DD (1976) Stability of fluid motions II. Springer, Berlin
14. Doering CR, Gibbon JD (1995) Applied analysis of the Navier–Stokes equations. Cambridge Texts in Applied Mathematics, Cambridge
15. Rajagopal KR, Růžička M, Srinivasa AR (1996) On the Oberbeck–Boussinesq approximation. Math Models Methods Appl Sci 6:1157–1167
16. Payne LE, Straughan B (1999) Effect of errors in the spatial geometry for temperature dependent Stokes flow. J Math Pure Appl 78:609–632
17. Kuehn TH, Goldstein RJ (1976) An experimental and theoretical study of natural convection in the annulus between horizontal concentric cylinders. J Fluid Mech 74:695–719
18. Lee DS, Rummler B (2002) The eigenfunctions of the Stokes operator in special domains. III. ZAMM 82:399–407
19. Passerini A, Růžička M, Thäter G (2006) Natural convection between two horizontal coaxial cylinders (submitted)
20. Galdi GP (1994) An introduction to the mathematical theory of the Navier–Stokes equations. Springer, Berlin